JACS
JOURNAL OF THE AMERICAN CHEMICAL SOCIETY
Article
pubs.acs.org/JACS

Highly Mesoporous Single-Crystalline Zeolite Beta Synthesized Using a Nonsurfactant Cationic Polymer as a Dual-Function Template

Jie Zhu,[†,#] Yihan Zhu,[‡] Liangkui Zhu,[§] Marcello Rigutto,[∥] Alexander van der Made,[∥] Chengguang Yang,[§] Shuxiang Pan,[†] Liang Wang,[†] Longfeng Zhu,[§] Yinying Jin,[†] Qi Sun,[†] Qinming Wu,[†] Xiangju Meng,*[,†] Daliang Zhang,*[,§] Yu Han,*[,‡] Jixue Li,[⊥] Yueying Chu,[&] Anmin Zheng,[&] Shilun Qiu,[§] Xiaoming Zheng,[†] and Feng-Shou Xiao*[,†]

[†]Key Lab of Applied Chemistry of Zhejiang Province, Department of Chemistry, Zhejiang University, Hangzhou 310028, China
[‡]Advanced Membranes and Porous Materials Center, Physical Sciences and Engineering Division, King Abdullah University of Science and Technology, Thuwal 23955-6900, Kingdom of Saudi Arabia
[§]State Key Laboratory of Inorganic Synthesis and Preparative Chemistry, Jilin University, Changchun 130012, China
[∥]Shell Technology Centre Amsterdam (STCA), CW-01-07, Grasweg 31, 1031 HW, Amsterdam, Netherlands
[⊥]Department of Materials Science and Engineering, Zhejiang University, Hangzhou 310027, China
[#]College of Biological, Chemical Sciences and Engineering, Jiaxing University, Jiaxing 314001, China
[&]State Key Laboratory of Magnetic Resonance and Atomic and Molecular Physics, Wuhan Institute of Physics and Mathematics, Chinese Academy of Sciences, Wuhan 430071, China

Supporting Information

ABSTRACT: Mesoporous zeolites are useful solid catalysts for conversion of bulky molecules because they offer fast mass transfer along with size and shape selectivity. We report here the successful synthesis of mesoporous aluminosilicate zeolite Beta from a commercial cationic polymer that acts as a dual-function template to generate zeolitic micropores and mesopores simultaneously. This is the first demonstration of a single nonsurfactant polymer acting as such a template. Using high-resolution electron microscopy and tomography, we discovered that the resulting material (Beta-MS) has abundant and highly interconnected mesopores. More importantly, we demonstrated using a three-dimensional electron diffraction technique that each Beta-MS particle is a single crystal, whereas most previously reported mesoporous zeolites are comprised of nanosized zeolitic grains with random orientations. The use of nonsurfactant templates is essential to gaining single-crystalline mesoporous zeolites. The single-crystalline nature endows Beta-MS with better hydrothermal stability compared with surfactant-derived mesoporous zeolite Beta. Beta-MS also exhibited remarkably higher catalytic activity than did conventional zeolite Beta in acid-catalyzed reactions involving large molecules.

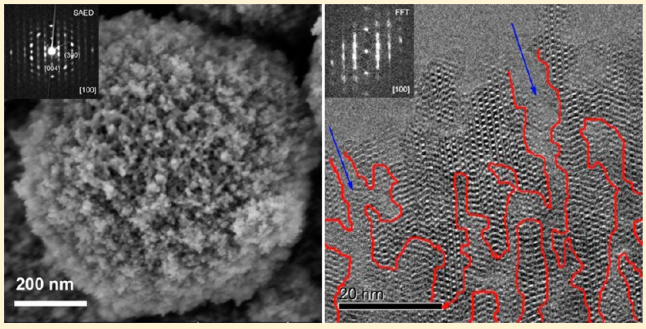

INTRODUCTION

Integrating mesopores into microporous zeolites would circumvent the diffusion limitation imposed by the small pore sizes of zeolites, making them applicable to catalysis involving large molecules.[1−27] In comparison with conventional methods for creating mesopores in zeolites, such as steaming, acid (or base) leaching, and chemical treatment, soft-templating routes that make use of large organic molecules, usually amphiphilic surfactants, as templates for mesopores allow more precise control of the mesopore size as well as better integrity of the zeolite structures by avoiding desilication or dealumination.[27−55] Initial attempts to design such routes were based on the use of a mixed template of surfactant molecules and small organic ions with the aim of simultaneously directing formation of mesoporous and microporous structures in one material. In most cases, however, only a mixture of zeolite crystals with an amorphous mesoporous material was obtained as a result of phase separation, due to the competition between the two different templating systems.[56−58] It is reasonable to expect that the most effective way to avoid phase separation would be the use of a two-in-one template with dual-structure-directing abilities on two different length scales. To this end, Ryoo's group developed a new class of surfactants featuring multiammonium groups with which they synthesized meso-structured (nanosheets) and mesoporous zeolites without the involvement of small templates.[47−54] Their work demonstrates the feasibility of directing the crystallization of a zeolite

Received: October 31, 2013
Published: January 22, 2014

dx.doi.org/10.1021/ja411117y | J. Am. Chem. Soc. 2014, 136, 2503−2510

framework with local functional groups of a large molecule, and it presents an effective synthetic strategy to create mesoporous zeolites.

All two-in-one (dual-function) templates developed to date have been surfactant based.[47−55] This is possibly driven by the long-pursued objective of synthesizing materials that possess ordered mesopores with crystalline zeolitic walls, given that surfactants are able to fabricate periodically ordered mesostructures through supermolecular self-assembly.[59] Although the tendency toward phase separation has been largely eliminated using a dual-function template, there still remain two major processes in the synthetic system, namely, condensation of alminosilicates and assembly of surfactant molecules, corresponding to generation of the zeolitic framework and the mesostructure, respectively. In general, these two processes are, both thermodynamically and kinetically, incompatible with each other. For one, the presence of mesopores induces severe strains in the crystalline zeolite frameworks; for the other, a mesostructure can be formed through supramolecular self-assembly in minutes, whereas crystallization of zeolites usually takes much longer. Consequently, it is difficult to achieve long-range order of both zeolitic and mesoporous structures simultaneously even when a dual-function template is used. For example, with surfactant-based dual-function templates, structural order on the mesoscale was realized, being lamellar[47] or hexagonal,[53] but only small zeolite grains rather than three-dimensionally continuous zeolitic frameworks were formed.

There seems to be an inherent trade-off between the zeolitic framework and the mesoporous structure in the degree of their structure ordering. The self-assembly ability of a surfactant-based dual-function template favors formation of an ordered mesostructure at the expense of continuity of the zeolitic framework. On the basis of this hypothesis, we propose that the opposite scenario, i.e., large zeolite single crystals containing disordered mesopores, may also be achievable if the interaction between the template molecules is minimized, by using, for example, a nonsurfactant template. The most important potential applications of mesoporous zeolites are as heterogeneous catalysts for oil conversion and refinement for which the ordering of the mesopores is not essential whereas the hydrothermal stability of the catalyst is crucial.[1,2,34,39,60−63] In this context, large zeolite single crystals with disordered mesopores may be advantageous over ordered mesostructured materials constituted from small polycrystalline zeolite grains, because in the latter case the junctions between differently oriented zeolite grains are vulnerable to hydrothermal treatment due to T−O−T (T is Si or Al) bond distortion or amorphous linkages.

Here, we demonstrate for the first time that a nonsurfactant cationic polymer can act as a dual-function template to synthesize mesoporous zeolite single crystals. As a proof-of-concept study, we use a commercial polymer, polydiallyldimethylammonium chloride (PDADMA) (Scheme 1). The abundant quaternary ammonium groups on the polymer act as a structure-directing agent (SDA) for the zeolite, which is similar to the cases of surfactant-based dual-function templates.[47−55] However, unlike surfactants, PDADMA does not self-assemble to form regular micelles or ordered structures due to the absence of hydrophobic segments. It therefore functions more simply as a "porogen" rather than as an actual SDA on the mesoscale, giving rise to disordered mesopores. In such a system, crystallization of the zeolite framework is not disrupted by template self-assembly, while the high flexibility of PDADMA molecules allows zeolite to crystallize into a thermodynamically more stable form, i.e., into a single crystal. With this strategy we successfully synthesized highly mesoporous single-crystalline zeolite Beta (denoted as Beta-MS). We characterized its single-crystalline nature and three-dimensionally (3-D) interconnected mesoporous network by high-resolution electron microscopy, electron diffraction, and tomography in both real space and reciprocal space. We found that Beta-MS possesses remarkable mesoporosity with a total pore volume as high as 0.89 cm^3/g, exceeding that of most previously reported mesoporous zeolites. The mesopore diameter can be tuned in the range of 4−10 nm by simply varying the molecular weight of PDADMA from 50 to 500 K. Beta-MS exhibited better hydrothermal stability than did surfactant-derived mesoporous zeolite Beta, as well as higher catalytic activity than did conventional zeolite Beta in large-molecule reactions. More significantly, its easy availability and low cost make PDADMA much more practical than specially designed, multistep synthesized surfactants for producing industrial catalysts.

Scheme 1. Chemical Structural Formula of (a) Polydiallyldimethylammonium Chloride and (b) Polydiallyldiethylammonium Chloride

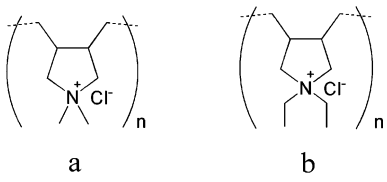

RESULTS AND DISCUSSION

Synthesis and Characterization of Beta-MS. Beta-MS was hydrothermally synthesized from an aluminosilicate gel with a typical composition of $45SiO_2/Al_2O_3/10Na_2O/2258H_2O/7.5$PDADMA (molecular weight $1−2 \times 10^5$). As indicated by scanning electron microscopy (SEM) images, Beta-MS consisted of relatively uniform particles with sizes ranging from 600 to 900 nm, and each particle had a highly mesoporous structure that could be easily identified on the particle surface (Figure 1a−c). The powder X-ray diffraction (PXRD) pattern showed characteristic peaks of *BEA-type zeolite (Figure 1d), indicating formation of microporous zeolite Beta crystals.[64] The coexistence of mesopores and micropores was confirmed by the N_2 sorption isotherm, which showed combined features of type I and type IV isotherms with two steep steps in the $P/P_0 < 0.01$ and $0.60 < P/P_0 < 0.90$ regions, corresponding to filling of the micropore volumes and capillary condensation in the mesopores, respectively (Figure 1e). The micropore diameters of Beta-MS were determined to be the same as conventional zeolite Beta with 12-membered ring channels (6.7 Å, Figure S1, Supporting Information), while the mesopore size distribution was centered at 8.4 nm (Figure 1f). The H1-type hysteresis loop of the isotherm suggests that the mesopores were interconnected through large openings without restriction on the capillary evaporation of the adsorbed gas. In comparison with conventional zeolite Beta synthesized with small tetraethylammonium cations, Beta-MS exhibited an apparently larger BET surface area (763 vs 554 m^2/g) and a higher total pore volume (0.89 vs 0.28 cm^3/g) owing to the contribution from a significant amount of mesopores (Table 1

dx.doi.org/10.1021/ja411117y | J. Am. Chem. Soc. 2014, 136, 2503−2510

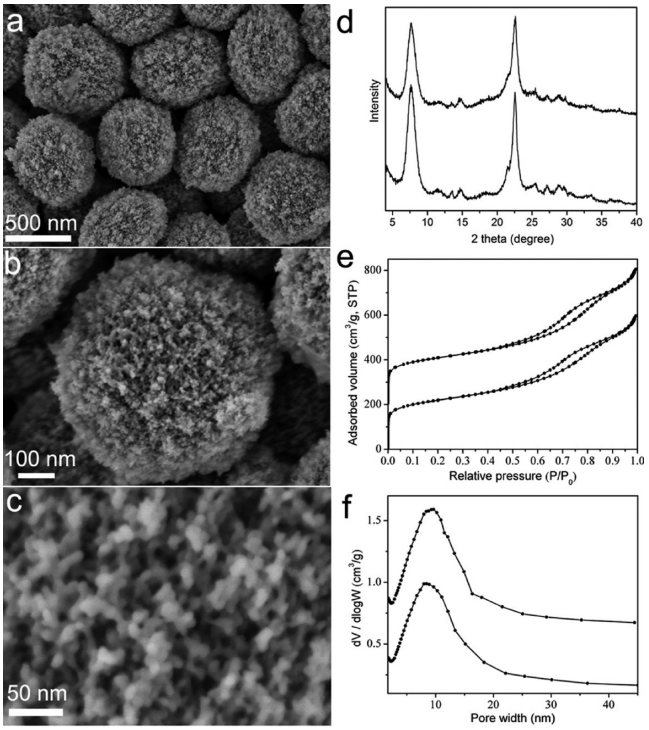

Figure 1. (a–c) SEM images of calcined Beta-MS at different magnifications. A pristine specimen without coating was used to image the original sample surface, and a low accelerating voltage of 1 KV was applied to minimize the charging effect. (d) XRD patterns, (e) N_2 sorption isotherms, and (f) pore size distribution curves of calcined Beta-MS before (lower) and after (upper) hydrothermal treatment with 100% steam flow at 973 K for 2 h.

and Figure S1, Supporting Information). Taking up a large proportion of the total pore volume, the mesopore (>1.5 nm) volume of Beta-MS was as high as 0.71 cm^3/g. This value surpasses that of most previous mesoporous zeolites,[8] comparable to those reported by Tsapatsis through confined synthesis.[17,20,21]

It is very interesting to note that despite being highly mesoporous, each Beta-MS particle is a single crystal. Selected-area electron diffraction (SAED) patterns of two individual particles are shown in Figure 2a and 2b, which contain discrete diffraction spots and can be indexed according to the *BEA-type zeolite structure in the [100] and [001] directions, respectively. The corresponding high-resolution transmission electron microscopy (HRTEM) images show lattice fringes with consistent orientations over the entire image regions (Figure 2), confirming that Beta-MS is comprised of single crystals rather than random aggregations of nanocrystals.[10,65,66]

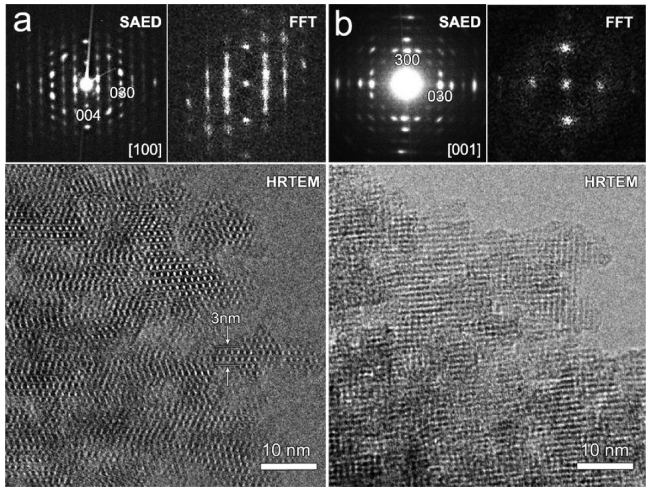

Figure 2. SAED patterns, HRTEM images, and corresponding FFT diffractograms of individual Beta-MS crystals taken along the (a) [100] and (b) [001] zone axes. Each SAED pattern was taken from an entire particle, demonstrating its single-crystalline nature. In the HRTEM image of the [100] zone axis, the 12-ring channels are well resolved as white dots and the characteristic stacking faults of the *BEA framework are observed. The presence of mesopores is also identified in the HRTEM images. FFTs confirm that the lattice fringes in each HRTEM image have consistent orientations over the entire image regions.

There are no amorphous components observed in Beta-MS by HRTEM. In the HRTEM image taken along the [100] zone axis at the crystal periphery where the specimen is ultrathin (Figure 2a), the 12-ring channels are well resolved as white dots and the characteristic stacking faults of the *BEA framework, i.e., the mixed ABAB... and ABCABC... stacking sequence of the 12-ring channels, are observed. The stacking faults explain the elongation of reflections observed in the SAED and fast Fourier transform (FFT) diffratograms (Figure 2a). Moreover, mesopores of 5–10 nm can be clearly identified in the HRTEM images, which break the single crystal into very small but continuous domains (Figure S2, Supporting Information). The smallest crystalline domain is about 3 nm in thickness, containing only two 12-ring channel layers (Figure 2a). High-angle-annular-dark-field scanning transmission electron microscopy (HAADF-STEM) was also used to characterize Beta-MS. It offered better image contrast than bright-field TEM for disordered mesopores in thick specimens, providing further evidence for the coexistence of a fully crystalline continuous zeolite framework and mesopores (Figure S3, Supporting Information).

SAED, HRTEM, and HAADF-STEM provide only two-dimensional (2-D) projection information of the specimen. A

Table 1. Textural Properties and Catalytic Performance of Different Catalysts before and after Steam Treatment at 973 K for 2 h

						yield (%)	conversion (%)	
sample	S_{BET} (m^2/g)	S_{mic}[b] (m^2/g)	V_{mic}[b] (cm^3/g)	mesopore size (nm)	V_{total}[c] (cm^3/g)	CBG	ABB[d]	CBH[e]
bulk Beta	554	528	0.25		0.28	33.4	25.0	29.0
Beta-MS	763	427	0.13	8.4	0.89	32.6	45.8	56.3
Beta-MS[a]	693	315	0.11	9.5	0.89	33.0	42.4	42.0
nano-BEA	833	352	0.12	4.2	1.33	32.6	46.0	53.8
nano-BEA[a]	774	134	0.05	4.5 and >20	2.22	28.1	36.0	38.8

[a]After treatment with 100% steam at 973 K for 2 h. [b]Surface areas and volumes of micropores (<1 nm) determined by the NLDFT method. [c]Single-point total pore volume at P/P_0 = 0.95. [d]Conversion of benzene. [e]Conversion of benzaldehyde.

dx.doi.org/10.1021/ja411117y | J. Am. Chem. Soc. 2014, 136, 2503–2510

recently developed technique, electron diffraction tomography (EDT),[67,68] allows three-dimensional (3-D) reciprocal space reconstruction of a crystal based on a series of SAED patterns. We used the EDT technique to characterize Beta-MS. In all, 435 SAED patterns were collected around an arbitrary axis at 0.2° intervals from a randomly selected Beta-MS crystal (Figure S4 and Movie si_002, Supporting Information). Although the big crystal size resulted in damped reflection peaks in the SAED patterns (Figure S4b, Supporting Information), strong reflections could still be recognized for reconstruction. The reconstruction process perfectly rendered a part of the reciprocal lattice of the zeolite *BEA framework (Movie si_003, Supporting Information), as represented by the three major projections along the a^*, b^*, and c^* directions (Figure 3a–c). This result unambiguously demonstrated the single-crystalline nature of Beta-MS. The a^* and b^* directions of an ideal *BEA structure are equivalent. However, the EDT reconstructed projection views of these two directions in Beta-MS were not completely identical (Figure 3b and 3c). Specifically, most reflections in the b^* projection appeared to be elongated with a flare angle of 10 ± 1.5° (Figure 3c). This observation suggests a certain degree of structural distortion in Beta-MS crystals, which is likely associated with the presence of highly dense mesopores.

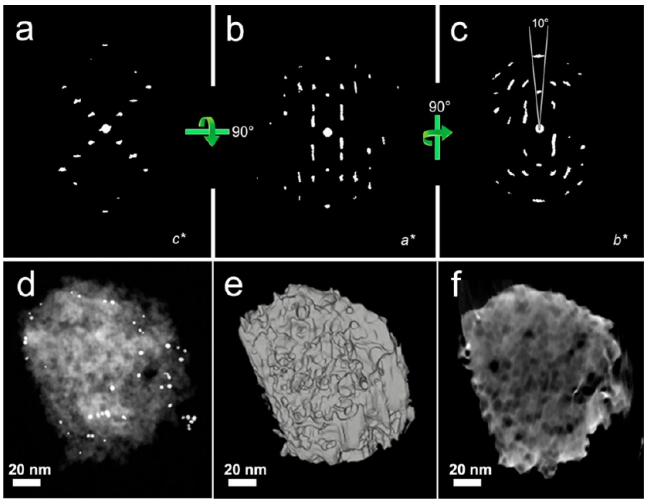

Figure 3. (a, b, and c) Reconstructed reciprocal lattice of Beta-MS from EDT projected along the c^*, a^*, and b^* directions, respectively. For the reciprocal space reconstruction, 435 SAED patterns were collected around an arbitrary axis at 0.2° intervals from a randomly selected Beta-MS crystal (Movie si_002, Supporting Information). (d) Representative HAADF-STEM image of Beta-MS selected from a tilting series over a range from −75° to +75° at regular intervals of 1° (Movie si_004, Supporting Information). The bright dots represent Au nanoparticles that were used as markers for image tracking during the tomography. (e) Reconstructed morphology of Beta-MS from HAADF-STEM tomography visualized by surface rendering. (f) A slice (2 nm thick) approximately normal to the [001] direction extracted from the reconstructed volume, clearly showing the presence of abundant mesopores within a Beta-MS crystal.

It should be noted that from a strict crystallographic point of view, describing the observed structure of Beta-MS as "single crystalline" may not be appropriate due to the intergrowth of different polymorphs, which is also common in bulk zeolite Beta. We here use the term "single crystalline" to distinguish Beta-MS from mesoporous zeolites constituted from randomly oriented nanocrystals. We notice that the majority of previously reported mesoporous zeolite single crystals are fabricated through hard-templating[10−12] or confined synthesis routes,[17,20,21] while there are very few examples by soft-templating synthesis.[35,69] In the latter cases, however, the zeolite topology is limited to MFI and the mesopores are to a great extent isolated from each other at a rather low density, resulting in limited mesoporosity (mesopore volume < 0.50 cm^3/g).

We further investigated the 3-D mesoporous structure of Beta-MS crystals by HAADF-STEM real-space tomography. In comparison with classic bright-field TEM tomography, HAADF-STEM tomography gives a much reduced diffraction contrast (unwanted in tomography) along with the enhanced Z contrast and is therefore suitable for reconstructing crystalline nanostructures. Given that the mesopores are disordered in arrangement, we chose a small fragment of Beta-MS crystal (~100 nm) for the tomography to gain reasonable contrast. Specifically, a series of STEM images was continuously acquired by tilting the specimen over a range from −75° to +75° at regular intervals of 1° (Movie si_004, Supporting Information). The image series was aligned and processed to reconstruct a "volume" that could be visualized through surface rendering or as a set of slices to show the "inner" local structures of the mesoporous crystal. One STEM image from the tilting series is shown in Figure 3d. Although the inner mesopores cannot be easily identified by surface rendering due to the intrinsic low contrast of this material, a highly mesoporous structure is clearly observed on the surface of the reconstructed 3-D image (Figure 3e). To visualize the distribution of the mesopores inside the crystal, we sliced the reconstructed volume (Movie si_005, Supporting Information). The result clearly demonstrates that there are three-dimensionally interconnected mesopores of very high density throughout the entire crystal. One representative slice is shown in Figure 3f.

Investigation of the Formation Mechanism of Beta-MS. Figure 4 showed ^1H and ^{13}C nuclear magnetic resonance (NMR) spectroscopy of as-synthesized Beta-MS. Notably, the spectra of the liquid phase obtained from as-synthesized Beta-MS exhibits peaks associated with aqueous PDADMA species. Moreover, ^{13}C NMR spectra demonstrate that the as-

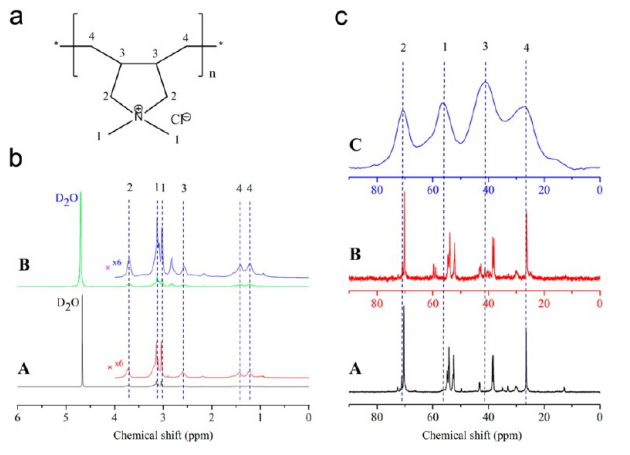

Figure 4. (a) Chemical structure of PDADMA. (b) ^1H NMR and (c) ^{13}C NMR spectra of (A) aqueous PDADMA, (B) the liquid phase obtained by dissolving as-synthesized Beta-MS with HF solution, followed by addition of D_2O, and (C) a solid sample of as-synthesized Beta-MS.

dx.doi.org/10.1021/ja411117y | J. Am. Chem. Soc. 2014, 136, 2503−2510

synthesized Beta-MS exhibits peaks associated with PDADMA species, although these peaks appearing in the solid sample are relatively weak and broad due to the low concentration of polymer species and magic angle spinning (MAS) measurements. These results indicate that PDADMA was indeed incorporated in Beta-MS during crystallization and that it acted as a dual-function template in its entirety, i.e., the PDADMA remained basically intact during the synthesis process (Figures S5 and S6, Supporting Information). Thermogravimetric analysis showed a marked weight loss (~28 wt %) in the region of 250−550 °C, corresponding to decomposition of PDADMA (Figure S7, Supporting Information). As demonstrated in earlier studies,[70,71] quaternary ammonium groups of a macromolecule can direct formation of microporous zeolitic structures if they have sufficient degrees of freedom. PDADMA has a high density of quaternary ammonium groups on a flexible polymer chain, and it is therefore a suitable SDA for the structure of zeolite. Meanwhile, the molecular agglomerates of PDADMA are incorporated in the zeolite structure during crystallization to play the role of a "porogen" on the mesoscale. As a nonsurfactant, PDADMA cannot form an ordered mesostructure through self-assembly, and the generated mesopores are therefore irregular in morphology and connectivity. On the other hand, PDADMA's strong interaction with aluminosilicates and its flexible polymer chains help to reduce the strain in the organic−inorganic composite structure, allowing formation of single crystals.

To a certain extent, Beta-MS resembles so-called "mesocrystals", which are single-crystalline or single-crystal-like inorganic structures that include organic macromolecules as defects.[72−74] Mesocrystals are formed through a nonclassical pathway, e.g., by the ordered assembly of well-defined building blocks. This is in striking contrast to the classical theory of crystallization, which is based on a "nucleation and growth" mechanism. To understand the formation process of Beta-MS, we investigated the intermediates at different crystallization times by means of PXRD, SEM, and TEM. As indicated by PXRD, no detectable crystalline structure was formed in the first 24 h after the start of the synthesis; the crystallinity of Beta-MS markedly increased between 36 and 72 h (Figure S8, Supporting Information). The SEM images show that irregular particles about 5−15 μm in size comprise the intermediates at 24 and 36 h. According to the XRD results, these particles are essentially amorphous. At 48 h after the start of the synthesis, a small number of crystals (600−900 nm) appeared on the surface of the bulky amorphous particles. More crystals were formed when the crystallization time was increased to 60 h. These crystals were connected to each other, and the formed aggregates were similar in size (~10 μm) to the original amorphous particles, suggesting that Beta-MS crystals nucleate from the amorphous particles. At the end of the synthesis (72 h), the amorphous components, which acted as a binder for the aggregated crystals, were completely consumed, leaving behind clean and isolated crystals as the final products (Figure S9, Supporting Information). According to TEM, the intermediate at 24 h was completely amorphous while it contained disordered mesopores (Figure S10a, Supporting Information), indicating that PDADMA consociated with the aluminosilicate species at the initial stage of the synthesis. Small crystalline grains embedded in the amorphous matrix were observed in the sample crystallized for 36 h, and with prolonged crystallization, they gradually grew into large crystals along with the disappearance of the amorphous particles. Throughout the crystallization process, there was no sign of an ordered assembly of preformed crystals, while disordered mesopores were observed in all intermediates (Figure S10, Supporting Information). Taken together, these results suggest that despite the inclusion of polymers, formation of Beta-MS single crystals still follows the classical "nucleation and growth" model of crystallization.

Evaluation of Catalytic Performance and Hydrothermal Stability. The combination of a highly interconnected 3-D mesoporous network and strongly acidic sites from the zeolite framework makes Beta-MS a promising solid acid catalyst, especially for converting bulky substrates. We evaluated the catalytic activities of Beta-MS with three reactions: condensation of benzaldehyde with glycerol (CBG), alkylation of benzene with benzyl alcohol (ABB), and condensation of benzaldehyde with hydroxyacetophenone (CBH) (Scheme 2). For comparison, a conventional zeolite

Scheme 2. Formulas of the Three Reactions Used for Evaluating Zeolite Beta-Based Catalysts[a]

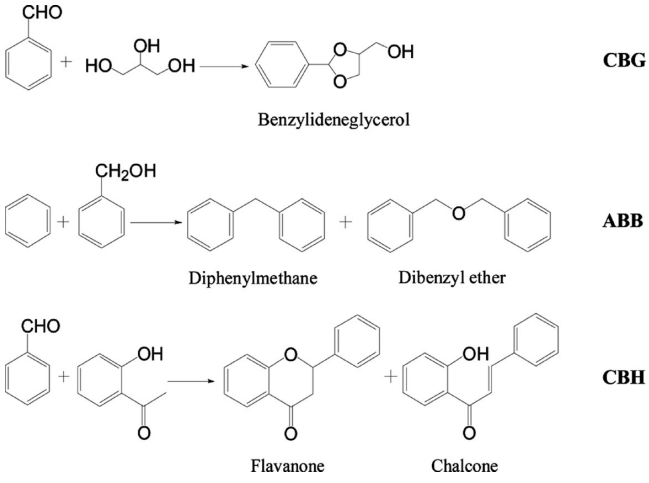

[a]From the top down are the condensation of benzaldehyde with glycerol, alkylation of benzene with benzyl alcohol, and condensation of benzaldehyde with hydroxyacetophenone.

Beta and a surfactant-derived mesoporous zeolite Beta (designated as nano-BEA) prepared according to the literature[53,54] were also tested with these reactions under the same conditions. As determined by N_2 sorption isotherms, nano-BEA has a smaller mesopore size (4.3 nm) and a larger BET surface area (833 m^2/g) than does Beta-MS. However, the most significant feature of nano-BEA that differentiates it from Beta-MS is that it consists of nanometer-sized zeolite crystals assembled in an irregular manner, as illustrated previously.[53,54] The three catalysts were prepared with similar Si/Al ratios (~11). They yielded almost the same amount of benzylideneglycerol (32−34%) in the CBG reaction (Table 1), where molecular diffusion is not a severe issue due to the relatively small sizes of the reactants and the product, while the activity of the catalyst is essentially determined by the strength of the acid site. This result suggested that incorporation of mesopores did not affect the intrinsic acidity of zeolite Beta, which was confirmed by NH_3 temperature-programmed desorption experiments (Figure S11, Supporting Information). The advantage of mesoporous zeolites became obvious when the reactions involved larger molecules. In the ABB reaction, for example, Beta-MS and nano-BEA converted ~46% of benzyl

dx.doi.org/10.1021/ja411117y | J. Am. Chem. Soc. 2014, 136, 2503−2510

alcohol, while conventional Beta converted only 25.0% of benzyl alcohol under the same reaction conditions. Likewise, Beta-MS and nano-BEA apparently exhibited higher activities than did conventional Beta for the CBH reaction (hydroxyacetophenone conversions 56.3% vs 53.8% vs 29.0%) (Table 1). The superior catalytic activities of Beta-MS and nano-BEA can be attributed to their highly mesoporous structures, which provide more accessible active sites and facilitate molecular diffusion of large substrates.

Although Beta-MS and nano-BEA demonstrate comparable catalytic activities, they differ in their hydrothermal stability. After being exposed to 100% steam flow at 973 K for 2 h, Beta-MS had a nearly unchanged XRD pattern (Figure 1d) and N_2 sorption isotherm (Figure 1e). Analysis of the isotherms based on the nonlocal density function theory (NLDFT) method shows that this harsh treatment resulted in the micropore volume of Beta-MS being decreased by ~15% from 0.13 to 0.11 cm^3/g and the average mesopore size slightly enlarged by about 1 nm (Figure 1f and Table 1). In contrast, the same steam treatment led to obvious changes in the N_2 sorption isotherm of nano-BEA (Figure S12, Supporting Information), in which the emergence of a marked capillary condensation step in the high relative pressure (>0.9) region suggests that large mesopores (>20 nm) were generated as a consequence of the destruction of the zeolite framework. This is confirmed by the fact that the micropore volume of nano-BEA drastically decreased by ~58% from 0.12 to 0.05 cm^3/g after treatment (Table 1). Due to the partial destruction of the zeolitic structure, the hydrothermally treated Beta-MS and nano-BEA both exhibited decreased catalytic activities, as compared with their untreated counterparts (Table 1). However, Beta-MS was apparently more active than nano-BEA after the steam treatment in all three reactions, although their original activities were rather close (Table 1). These results demonstrate that the high stability of Beta-MS allows it to effectively retain active sites during hydrothermal treatment, which is an important criterion for catalysts with potential use in petrochemical applications.

Synthesis of Beta-MS with Different Polymers. The mesopore size of as-synthesized Beta-MS can be tuned in the range of 4−10 nm, as determined by N_2 adsorption measurements, by simply varying the molecular weight of PDADMA from 50 to 500 K; the obtained materials all exhibit single-crystal-like electron diffraction patterns, indicating that the molecular weight of the template has little effect on zeolite crystallization (Figure S13, Supporting Information). More precise control of the mesopore size can be achieved by mixing PDADMA of different molecular weights for synthesis (Figure S14, Supporting Information). Moreover, we found that another nonsurfactant quaternary ammonium cationic polymer, polydiallyldiethylammonium chloride (Scheme 1), is also capable of directing the synthesis of mesoporous single-crystalline zeolite Beta (Figure S15, Supporting Information). These results suggest that the present method may be generalized for preparing mesoporous zeolite single crystals of other topologies by rationally designing the functional groups on the nonsurfactant polymer.

SUMMARY AND CONCLUSION

We developed a new strategy for synthesizing mesoporous zeolites. As an example, we synthesized single-crystalline zeolite Beta with highly interconnected mesopores using a nonsurfactant cationic polymer as a dual-function template. We proposed that the use of this nonsurfactant template is the key to obtaining the single-crystalline zeolite framework, which in turn accounts for the excellent hydrothermal stability of this material. Another obvious advantage of our synthesis method is that the required templates are low-cost, commercially available polymers, which makes large-scale production of our mesoporous zeolites possible. We demonstrated that the combination of high-density mesopores and zeolitic frameworks gave rise to superior catalytic performance for reactions involving large molecules. In addition to heterogeneous catalysis, mesoporous zeolite single crystals have other potential applications. For example, they are ideal building blocks for fabricating hierarchically porous membranes; when arranged with uniform orientations, they would provide well-aligned micropores throughout the membrane to achieve highly selective separation or catalysis via the molecular sieve effect. Relevant studies are currently underway.

METHOD

Synthesis of Beta-MS. Beta-MS samples with Si/Al ratios at 9.0−12.0 were hydrothermally synthesized from aluminosilicate gels with Si/Al ratios at 22−45. A typical composition is $45SiO_2/Al_2O_3/10Na_2O/2258H_2O/7.5$PDADMA. In a typical synthesis of Beta-MS, 0.08 g of $NaAlO_2$ and 0.3 g of NaOH were dissolved in 12.1 mL of H_2O, followed by addition of 2 g of PDADMA ($1-2 \times 10^5$, 20 wt % in water) with stirring for 0.5 h. When a clear solution was formed, 0.935 g of fumed silica was added to the solution. After stirring for 12 h, the resulting gel was transferred into an autoclave for crystallization at 180 °C for 96 h. The obtained powder was collected by filtration at room temperature, dried at 100 °C, and calcined at 550 °C for 5 h to remove the organic template. Beta-MS samples with different mesopore sizes were synthesized by following the same procedure but using PDADMA of different molecular weights.

ASSOCIATED CONTENT

Supporting Information

Video information files for the single-crystalline nature of Beta-MS by EDT (Movie si_002, Movie si_003) and the 3-D mesoporous structure of Beta-MS by HAADF-STEM (Movie si_004, Movie si_005); PDF document containing the synthesis procedures of conventional bulk zeolite Beta and nano-BEA, details of materials characterization, and conditions of catalytic reactions. This material is available free of charge via the Internet at http://pubs.acs.org.

AUTHOR INFORMATION

Corresponding Authors

mengxj@zju.edu.cn
zhangdaliang@jlu.edu.cn
yu.han@kaust.edu.sa
fsxiao@zju.edu.cn

Notes

The authors declare no competing financial interest.

ACKNOWLEDGMENTS

This research was supported by the National Natural Science Foundation of China (Grants 11227403, 21201076, 91022030, 21333009), Fundamental Research Funds for the Central Universities (2013XZZX001), Shell Company, and the Competitive Research Grant to Y.H. from King Abdullah University of Science and Technology. Y.H.Z. is supported by the Sabic Post-doc Fellowship.

REFERENCES

(1) Corma, A. *Chem. Rev.* **1997**, *97*, 2373−2401.
(2) Davis, M. E. *Nature* **2002**, *417*, 813−821.
(3) Cundy, C. S.; Cox, P. A. *Chem. Rev.* **2003**, *103*, 663−702.
(4) Tao, Y.; Kanoh, H.; Abrams, L.; Kaneko, K. *Chem. Rev.* **2006**, *106*, 896−910.
(5) Perez-Ramirez, J.; Christensen, C. H.; Egeblad, K.; Christensen, C. H.; Groen, J. C. *Chem. Soc. Rev.* **2008**, *37*, 2530−2542.
(6) Serrano, D. P.; Escola, J. M.; Pizarro, P. *Chem. Soc. Rev.* **2008**, *42*, 4004−4035.
(7) Morris, R. E. *Top. Catal.* **2010**, *53*, 19−20.
(8) Moller, K.; Bein, T. *Chem. Soc. Rev.* **2013**, *42*, 3689−3707.
(9) Holland, B. T.; Abrams, L.; Stein, A. *J. Am. Chem. Soc.* **1999**, *121*, 4308−4309.
(10) Jacobsen, C. J. H.; Madsan, C.; Houzvicka, J.; Schmidt, I.; Carlsson, A. *J. Am. Chem. Soc.* **2000**, *122*, 7116−7117.
(11) Tao, Y.; Kanoh, H.; Kaneko, K. *J. Am. Chem. Soc.* **2003**, *125*, 6044−6045.
(12) Christensen, C. H.; Johannsen, K.; Schmidt, I.; Christensen, C. H. *J. Am. Chem. Soc.* **2003**, *125*, 13370−13371.
(13) Zou, X.; Conradsson, T.; Klingstedt, M.; Dadachov, M. S.; O'Keeffe, M. *Nature* **2005**, *437*, 716−719.
(14) Groen, J. C.; Peffer, L. A. A.; Moulijn, J. A.; Perez-Ramirez, J. *Chem.—Eur. J.* **2005**, *11*, 4983−4994.
(15) Serrano, D. P.; Aguado, J.; Escola, J. M.; Rodriguez, J. M.; Peral, A. *Chem. Mater.* **2006**, *18*, 2462−2464.
(16) Groen, J. C.; Zhu, W. D.; Brouwer, S.; Huynink, S. J.; Kapteijn, F.; Moulijn, J. A.; Perez-Ramirez, J. *J. Am. Chem. Soc.* **2007**, *129*, 355−360.
(17) Fan, W.; Snyder, M. A.; Kumar, S.; Lee, P. S.; Yoo, W. C.; McCormick, A. V.; Penn, R. L.; Stein, A.; Tsapatsis, M. *Nat. Mater.* **2008**, *7*, 984−991.
(18) Yoo, W. C.; Kumar, S.; Penn, R. L.; Tsapatsis, M.; Stein, A. *J. Am. Chem. Soc.* **2009**, *131*, 12377−12383.
(19) Ren, X. Y.; Li, Y.; Pan, Q. H.; Yu, J. H.; Xu, R. R.; Xu, Y. *J. Am. Chem. Soc.* **2009**, *131*, 14128−14129.
(20) Lee, P.-S.; Zhang, X. Y.; Stoeger, J. A.; Malek, A.; Fan, W.; Kumar, S.; Yoo, W. C.; Hashimi, S. A.; Penn, R. L.; Stein, A.; Tsapatsis, M. *J. Am. Chem. Soc.* **2011**, *133*, 493−502.
(21) Chen, H. Y.; Wydra, J.; Zhang, X. Y.; Lee, P. S.; Wang, Z. P.; Fan, W.; Tsapatsis. *J. Am. Chem. Soc.* **2011**, *133*, 12390−12393.
(22) Jiang, J. X.; Jorda, J. L.; Yu, J. H.; Baumes, L. A.; Mugnaioli, E.; Diaz-Cabanas, M. J.; Kolb, U.; Corma, A. *Science* **2011**, *333*, 1131−1134.
(23) Moller, K.; Yilmaz, B.; Jacubinas, R. M.; Muller, U.; Bein, T. *J. Am. Chem. Soc.* **2011**, *133*, 5284−5295.
(24) Mollen, K.; Yilmaz, B.; Bein, T. *Chem.—Eur. J.* **2012**, *18*, 7671−7674.
(25) Zhang, X. Y.; Liu, D. X.; Xu, D. D.; Asahina, S.; Cychosz, K. A.; Agrawal, K. V.; Al Wahedi, Y.; Bhan, A.; Al Hashimi, S.; Terasaki, O.; Thommes, M.; Tsapatsis, M. *Science* **2012**, *336*, 1684−1687.
(26) Li, B.; Sun, B.; Qian, X. F.; Li, W.; Wu, Z. X.; Sun, Z. K.; Qiao, M. H.; Duke, M.; Zhao, D. Y. *J. Am. Chem. Soc.* **2013**, *135*, 1181−1184.
(27) Na, K.; Choi, M.; Ryoo, R. *Microporous Mesoporous Mater.* **2013**, *166*, 3−19.
(28) Choi, M.; Cho, H. S.; Srivastava, R.; Venkatesan, C.; Choi, D.-H.; Ryoo, R. *Nat. Mater.* **2006**, *5*, 718−723.
(29) Srivastava, R.; Choi, M.; Ryoo, R. *Chem. Commun.* **2006**, 4489−4491.
(30) Kim, J.; Choi, M.; Ryoo, R. *J. Catal.* **2010**, *269*, 219−228.
(31) Wang, H.; Pinnavaia, T. J. *Angew. Chem., Int. Ed.* **2006**, *45*, 7603−7606.
(32) Park, D. H.; Kim, S. S.; Wang, H.; Pinnavaia, T. J.; Papapetrou, M. C.; Lappas, A. A.; Triantafyllidis, K. S. *Angew. Chem., Int. Ed.* **2009**, *48*, 7645−7648.
(33) Xiao, F.-S.; Wang, L. F.; Yin, C. Y.; Lin, K. F.; Di, Y.; Li, J.; Xu, R.; Su, D. S.; Schlogl, R.; Yokoi, T.; Tatsumi, T. *Angew. Chem., Int. Ed.* **2006**, *45*, 3090−3093.
(34) Fu, W.; Zhang, L.; Tang, T.; Ke, Q.; Wang, S.; Hu, J.; Fang, G.; Li, J.; Xiao, F.-S. *J. Am. Chem. Soc.* **2011**, *133*, 15346−15349.
(35) Liu, F. J.; Willhammar, T.; Wang, L.; Zhu, L. F.; Sun, Q.; Meng, X. J.; Carrillo-Cabrera, W.; Zou, X. D.; Xiao, F.-S. *J. Am. Chem. Soc.* **2012**, *134*, 4557−4560.
(36) Reichinger, M.; Schmidt, W.; Narkhede, V. V.; Zhang, W. P.; Gies, H.; Grunert, W. *Microporous Mesoporous Mater.* **2012**, *164*, 21−31.
(37) Chen, L. H.; Li, X. Y.; Tian, G.; Li, Y.; Rooke, J. C.; Zhu, G. S.; Qiu, S. L.; Yang, X. Y.; Su, B.-L. *Angew. Chem., Int. Ed.* **2011**, *50*, 11156−11161.
(38) Yang, X. Y.; Tian, G.; Chen, L. H.; Li, Y.; Tooke, J. C.; Wei, Y. X.; Liu, Z. M.; Deng, Z.; Can Tendeloo, G.; Su, B. L. *Chem.—Eur. J.* **2011**, *17*, 14978−14995.
(39) Sun, Y. Y.; Prins, R. *Angew. Chem., Int. Ed.* **2008**, *47*, 8478−8481.
(40) Sun, Y. Y.; Prins, R. *Appl. Catal. A: Gen.* **2008**, *336*, 11−16.
(41) Zhu, H. B.; Liu, Z. C.; Kong, D. J.; Wang, Y. D.; Xie, Z. K. *J. Phys. Chem. .* **2008**, *112*, 17257−17264.
(42) Hua, J.; Han, Y. *Chem. Mater.* **2009**, *21*, 2344−2348.
(43) Gu, F. N.; Wei, F.; Yang, J. Y.; Lin, N.; Lin, W. G.; Lin, Y.; Zhu, J. H. *Chem. Mater.* **2010**, *22*, 2442−2450.
(44) Zhou, J. A.; Hua, Z. L.; Cui, X. Z.; Ye, Z. Q.; Cui, F. M.; Shi, J. L. *Chem. Commun.* **2010**, *46*, 4994−4996.
(45) Zhou, X. X.; Chen, H. R.; Zhu, Y.; Song, Y. D.; Chen, Y.; Wang, Y. X.; Gong, Y.; Zhang, G. B.; Shu, Z.; Cui, X. Z.; Zhao, J. J.; Shi, J. L. *Chem.—Eur. J.* **2013**, *19*, 10017−10023.
(46) Liu, J.-Y.; Wang, J.-G.; Li, N.; Zhao, H.; Zhou, H.-J.; Sun, P.-C.; Chen, T.-H. *Langmuir* **2012**, *28*, 8600−8607.
(47) Choi, M.; Na, K.; Kim, J.; Sakamoto, Y.; Terasaki, O.; Ryoo, R. *Nature* **2009**, *461*, 246−249.
(48) Na, K.; Choi, M.; Park, W.; Sakamoto, Y.; Terasaki, O.; Ryoo, R. *J. Am. Chem. Soc.* **2010**, *132*, 4169−4177.
(49) Jung, J.; Jo, C.; Cho, K.; Ryoo, R. *J. Mater. Chem.* **2012**, *22*, 4637−4640.
(50) Park, W.; Yu, D.; Na, K.; Jelfs, K. E.; Slater, B.; Sakamoto, Y.; Ryoo, R. *Chem. Mater.* **2011**, *23*, 5131−5137.
(51) Na, K.; Jo, C.; Kun, J.; Ahn, W. S.; Ryoo, R. *ACS Catal.* **2011**, *1*, 901−907.
(52) Seo, Y.; Lee, S.; Jo, C.; Ryoo, R. *J. Am. Chem. Soc.* **2013**, *135*, 8806−8809.
(53) Na, K.; Jo, C.; Kim, J.; Cho, K.; Jung, J.; Seo, Y.; Messinger, R. J.; Chmelka, B. F.; Ryoo, R. *Science* **2011**, *333*, 328−332.
(54) Cho, K.; Na, K.; Kim, J.; Terasaki, O.; Ryoo, R. *Chem. Mater.* **2012**, *24*, 2733−2738.
(55) Kore, R.; Sridharkrishna, R.; Srivastava, R. *RSC. Adv.* **2013**, *3*, 1317−1322.
(56) Huang, L. M.; Guo, W. P.; Deng, P.; Xue, Z. Y.; Li, Q. Z. *J. Phys. Chem. B.* **2000**, *104*, 2817−2823.
(57) Guo, W. P.; Huang, L. M.; Deng, P.; Xue, Z. Y.; Li, Q. Z. *Microporous Mesoporous Mater.* **2001**, *44*, 427−434.
(58) Karlsson, A.; Stoker, M.; Schmidt, R. *Microporous Mesoporous Mater.* **1999**, *27*, 181−192.
(59) Moller, K.; Bein, T. *Science* **2011**, *333*, 297−298.
(60) de Jong, K. P.; Zecevic, J.; Friedrich, H.; de Jongh, P. E.; Bulut, M.; van Donk, S.; Kenmogne, R.; Finiels, A.; Hulea, V.; Fajula, F. *Angew. Chem., Int. Ed.* **2010**, *49*, 10074−10078.
(61) Mitchell, S.; Michels, N. L.; Kunze, K.; Perez-Ramirez, J. *Nature Chem.* **2012**, *4*, 825−831.
(62) Martinez, C.; Verboekend, D.; Perez-Ramirez, J.; Corma, A. *Catal. Sci. Technol.* **2013**, *3*, 972−981.
(63) Corma, A.; Grande, M. S.; Gonzalez-Alfaro, V.; Orchilles, A. V. *J. Catal.* **1996**, *159*, 375−382.
(64) Baerlocher, Ch.; McCusker, L. B.; Olson, D. H. *Atlas of Zeolite Framework Types*, 6th ed.; Elsevier: Amsterdam, 2007.
(65) Schmidt, I.; Boisen, A.; Gustavsson, E.; Stahl, K.; Pehrson, S.; Dahl, S.; Carlsson, A.; Jacobsen, C. J. H. *Chem. Mater.* **2001**, *13*, 4416−4418.

(66) Boisen, A.; Schmidt, I.; Carlsson, A.; Dahl, S.; Brorson, M.; Jacobsen, C. J. H. *Chem. Commun.* **2003**, 958−959.
(67) Kolb, U.; Gorelik, T.; Kübel, C.; Otten, M. T.; Hubert, D. *Ultramicroscopy* **2007**, *107*, 507−513.
(68) Zhang, D. L.; Oleynikov, P.; Hovmöller, S.; Zou, X. D. *Z. Kristallogr.* **2010**, *225*, 94−102.
(69) Tao, H. X.; Li, C. L.; Ren, J. W.; Wang, Y. Q.; Lu, G. Z. *J. Solid State Chem.* **2011**, *184*, 1820−1827.
(70) Daniels, R. H.; Kerr, G. T.; Rollmann, L. D. *J. Am. Chem. Soc.* **1978**, *100*, 3097−3100.
(71) Jackowski, A.; Zones, S. I.; Hwang, S. J.; Burton, A. W. *J. Am. Chem. Soc.* **2009**, *131*, 1092−1100.
(72) Colfen, H.; Antonietti, M. *Angew. Chem., Int. Ed.* **2005**, *44*, 5576−5591.
(73) Meldrum, F. C.; Colfen, H. *Chem. Rev.* **2008**, *108*, 4332−4432.
(74) Wu, X. L.; Xiong, S. J.; Liu, Z.; Chen, J.; Shen, J. C.; Li, T. H.; Wu, P. H.; Chu, P. K. *Nat. Nanotechnol.* **2011**, *6*, 102−105.